



**HAL**  
open science

# Climate Extreme Versus Carbon Extreme: Responses of Terrestrial Carbon Fluxes to Temperature and Precipitation

Shufen Pan, Jia Yang, Hanqin Tian, Hao Shi, Jinfeng Chang, Philippe Ciais, Louis Francois, Katja Frieler, Bojie Fu, Thomas Hickler, et al.

► **To cite this version:**

Shufen Pan, Jia Yang, Hanqin Tian, Hao Shi, Jinfeng Chang, et al.. Climate Extreme Versus Carbon Extreme: Responses of Terrestrial Carbon Fluxes to Temperature and Precipitation. Journal of Geophysical Research: Biogeosciences, 2020, 125 (4), pp.e2019JG005252. 10.1029/2019JG005252 . hal-02948763

**HAL Id: hal-02948763**

**<https://hal.science/hal-02948763>**

Submitted on 21 Jun 2021

**HAL** is a multi-disciplinary open access archive for the deposit and dissemination of scientific research documents, whether they are published or not. The documents may come from teaching and research institutions in France or abroad, or from public or private research centers.

L'archive ouverte pluridisciplinaire **HAL**, est destinée au dépôt et à la diffusion de documents scientifiques de niveau recherche, publiés ou non, émanant des établissements d'enseignement et de recherche français ou étrangers, des laboratoires publics ou privés.



## Responses of terrestrial carbon fluxes to temperature and precipitation: carbon extreme versus climate extreme

Shufen Pan<sup>1\*</sup>, Jia Yang<sup>1,2\*</sup>, Hanqin Tian<sup>1#</sup>, Hao Shi<sup>1,3</sup>, Jinfeng Chang<sup>4</sup>, Philippe Ciais<sup>4</sup>, Louis Francois<sup>5</sup>, Katja Frieler<sup>6</sup>, Bojie Fu<sup>3</sup>, Thomas Hickler<sup>7,8</sup>, Akihiko Ito<sup>9</sup>, Kazuya Nishina<sup>9</sup>, Sebastian Ostberg<sup>6</sup>, Christopher P.O. Reyer<sup>6</sup>, Sibyll Schaphoff<sup>6</sup>, Jörg Steinkamp<sup>7</sup>, Fang Zhao<sup>6</sup>

1. International Center for Climate and Global Change Research, School of Forestry and Wildlife Sciences, Auburn University, Auburn, Alabama, USA
2. Department of Forestry, Mississippi State University, Mississippi State, Mississippi, USA
3. Research Center for Eco-Environmental Sciences, State Key Laboratory of Urban and Regional Ecology, Chinese Academy of Sciences, Beijing, China
4. Laboratoire des Sciences du Climat et de l'Environnement, Gif-sur-Yvette, France
5. UR – SPHERES, Université de Liège, B-4000 Liège, Belgium.
6. Potsdam Institute for Climate Impact Research (PIK), Member of the Leibniz Association, P.O. Box 60 12 03, D-14412 Potsdam, Germany
7. Senckenberg Biodiversity and Climate Research Centre (BiK-F), Senckenberganlage 25, 60325 Frankfurt am Main, Germany.
8. Goethe University, Department of Physical Geography, Altenhöferallee 1, 60438 Frankfurt am Main, Germany.
9. National Institute for Environmental Studies, 16-2 Onogawa, Tsukuba, Ibaraki, 305-8506, Japan.

\* Equal contribution

#Corresponding author:

Dr. Hanqin Tian, E-mail: [tianhan@auburn.edu](mailto:tianhan@auburn.edu)

Revised Manuscript submitted (February 2020)  
*Journal of Geographical Research*

This article has been accepted for publication and undergone full peer review but has not been through the copyediting, typesetting, pagination and proofreading process which may lead to differences between this version and the Version of Record. Please cite this article as doi: 10.1029/2019JG005252

## Key Points

- Impacts of temperature or precipitation extremes on carbon fluxes could be amplified due to their interactive effects.
- Hot extremes lead to a larger carbon loss in tropics while ecosystems in the arid zones show the largest sensitivity to precipitation.
- Models simulated larger sensitivity of ecosystem productivity to precipitation than satellite product, particularly in tropics.

## Abstract

Carbon fluxes at the land-atmosphere interface are strongly influenced by weather and climate conditions. Yet, what is usually known as “climate extremes” does not always translate into very high or low carbon fluxes or so-called “carbon extremes”. To reveal the patterns of how climate extremes influence terrestrial carbon fluxes, we analyzed the inter-annual variations in ecosystem carbon fluxes simulated by the Terrestrial Biosphere Model (TBMs) in the Inter-Sectoral Impact Model Intercomparison Project. At the global level, TBMs simulated reduced ecosystem Net Primary Productivity (NPP) ( $18.5 \pm 9.3 \text{ g C m}^{-2} \text{ yr}^{-1}$ ), but enhanced heterotrophic respiration (Rh) ( $7 \pm 4.6 \text{ g C m}^{-2} \text{ yr}^{-1}$ ) during extremely hot events. TBMs also simulated reduced NPP ( $60.9 \pm 24.4 \text{ g C m}^{-2} \text{ yr}^{-1}$ ) and reduced Rh ( $16.5 \pm 11.4 \text{ g C m}^{-2} \text{ yr}^{-1}$ ) during extreme dry events. Influences of precipitation extremes on terrestrial carbon uptake were larger in the arid/semi-arid zones than other regions. During hot extremes, ecosystems in the low latitudes experienced a larger reduction in carbon uptake. However, a large fraction of carbon extremes did not occur in concert with either temperature or precipitation extremes. Rather these carbon extremes are likely to be caused by the interactive effects of the concurrent temperature and precipitation anomalies. The interactive effects showed considerable spatial variations with the largest effects on NPP in South America and Africa. Additionally, TBMs simulated a stronger sensitivity of ecosystem productivity to precipitation than satellite estimates. This study provides new insights into the complex

ecosystem responses to climate extremes, especially emergent properties of carbon dynamics resulting from compound climate extremes.

### **Plain Language Summary**

Terrestrial ecosystems sequester a large amount of carbon dioxide from the atmosphere, which helps to mitigate climate warming. Climate extremes, such as droughts and heatwaves, play a significant role in determining the capacity of land ecosystems in carbon uptake. In the past decades, terrestrial biosphere models have been widely used to investigate the magnitude and variations of carbon fluxes between land and the atmosphere. In this study, we attempted to understand how model-simulated carbon fluxes respond to climate anomalies and extremes at the global level and across regions. Analysis of model simulations showed significant spatial variations in the sensitivity of carbon fluxes to climate variations. Interestingly, concurrences of abnormal temperature and precipitation could have stronger impacts on carbon fluxes than individual temperature or precipitation event. This study is important for better understanding climate extreme impacts on ecosystem dynamics and the global carbon cycle.

## **Keywords:**

Climate extremes; Carbon extremes; Terrestrial Biosphere Model; Model ensemble; Satellite remote sensing

## **1. Introduction**

Terrestrial ecosystems remove atmospheric carbon dioxide (CO<sub>2</sub>) via photosynthesis and release most of the previously fixed carbon to the atmosphere via autotrophic and heterotrophic respirations and land disturbances (Ciais et al., 2014). As reported by the most recent global carbon project (Le Quéré et al., 2018), the terrestrial CO<sub>2</sub> sink was  $3.2 \pm 0.8$  Pg C yr<sup>-1</sup> during the period of 2007-2018, which offset about 1/3 of the anthropogenic carbon emissions. It is worth noting that both ecosystem carbon sequestration and emission present significant inter-annual variations mainly due to the influences of precipitation and temperature fluctuations (Ahlström et al., 2015; Beer et al., 2010; Pan et al. 2015), and explain most of the inter-annual changes of the atmospheric CO<sub>2</sub> concentration (Ahlström et al., 2015; Jung et al., 2017; Le Quéré et al., 2018). Therefore, a better understanding of the relationships between climate and terrestrial carbon fluxes on the inter-annual scale is important to project future climate-carbon feedbacks even though decadal and centennial scales may elicit different processes in the carbon cycle.

According to the IPCC SREX special report on extreme events (Seneviratne et al., 2012), a climate extreme is defined as “the occurrence of a value of a weather or climate variable above (or below) a threshold value near the upper (or lower) ends of the range of observed values of the variable”. Extreme climate events include but are not limited to droughts, floods, heatwaves, frosts and strong winds, which hold the potential to greatly alternate ecosystem physiological processes, structure, composition, and thus carbon balance (Frank et al., 2015). Climate extremes have dual influences on terrestrial carbon fluxes through

immediate changes in environmental controls on photosynthesis and respiration rates, and a legacy effect on carbon pools (Reichstein et al., 2013; Schwalm et al., 2017). At present, the impacts of extreme droughts on carbon cycling have been widely investigated. For example, the 2003 European drought was estimated to reduce gross primary productivity (GPP) by 30% and result in a strong continent-wide carbon source (Ciais et al., 2005); the 2010 Amazon drought reduced net primary production (NPP) in forested area by about 7% (Potter et al., 2011); the turn of the century drought (2000-2004) in western North America reduced the carbon sink by 30-298 Tg C yr<sup>-1</sup> (Schwalm et al., 2012). Global impacts of extreme drought events on carbon cycling have been examined by modeling, satellite-based estimates, and statistical extrapolations (e.g. Schwalm et al., 2010, 2017; Zscheischler et al., 2014a). However, knowledge of the impacts of other climate extremes, such as extremely hot, extremely cold, and extremely wet events, on terrestrial carbon fluxes is still limited at both regional and global scales.

Climate extremes may lead to large variations in terrestrial carbon fluxes, but do not necessarily result in carbon extremes (Reyer et al., 2013), which have been found to dominate the inter-annual variations of global carbon fluxes (Zscheischler et al., 2014b). To emphasize the climate impacts on the biosphere, a biosphere-relevant climate extreme is defined as “climate conditions where an ecosystem function is out of a defined extreme percentile threshold over a certain period” (Reichstein et al., 2013). As such, the method of “backward assessment”, which first identifies extreme ecosystem carbon flux anomalies and then relates them to single or multiple climate variables, has been developed to examine biosphere-relevant climate extremes and their ecological consequences. Previous research found that negative global GPP extremes can be attributed to water scarcity in a large part of the global land area (Zscheischler et al., 2014b). Yet, challenges remain for a rigorous global quantification of carbon cycle extremes (including carbon sequestration, emission, and net carbon budget) and their related climate conditions (Frank et al., 2015).

Investigation of extreme climate impacts on carbon fluxes should consider the sensitivity of carbon fluxes to climate variables across vegetation types and climate zones. Carbon fluxes in semi-arid regions in the Southern Hemisphere are particularly sensitive to precipitation anomalies and dominate the inter-annual anomalies of the global terrestrial carbon sink (Ahlström et al., 2015; Poulter et al., 2014); in contrast, forests in many humid regions seem to be less affected by precipitation variations or even green up during periods with reduced water supply (Knapp & Smith, 2001; Saleska et al., 2007; Vicente-Serrano et al., 2013; Yang et al., 2018). Such contrasting responses highlight the importance of studies regarding the precipitation sensitivity of land ecosystems across various climate zones (Wu et al., 2018). Meanwhile, responses of different carbon fluxes to climate variations diverge in magnitude. Based on site-level observations, Shi et al. (2014) found that the sensitivity of GPP to precipitation is generally higher than that of ecosystem respiration. At the global scale, the sensitivity of GPP to precipitation is reported to be about 50% larger than that of ecosystem respiration (Schwalm et al., 2010). However, the sensitivity of different components of carbon fluxes to temperature has not been systematically evaluated at the global scale, which limits our understanding of the carbon dynamics under extreme temperature events.

Therefore, there is an important need to evaluate how global terrestrial ecosystems respond to climate variations and extremes. Terrestrial Biosphere Models (TBMs) are an essential tool to investigate carbon exchanges between land and the atmosphere, and understand the impacts of global climate change on land ecosystems (Le Quéré et al., 2018). In this study, we analyzed the impacts of climate extremes on terrestrial ecosystem carbon fluxes in the 40 years between 1971 and 2010, based on 19 sets of model simulations combining three climate datasets and seven TBMs from the Inter-Sectoral Impact Model Intercomparison Project (ISIMIP) Phase 2a (<https://www.isimip.org/protocol/#isimip2a>). The specific objectives of this study are to (1) evaluate the spatial patterns of the sensitivity of land

ecosystem carbon fluxes to inter-annual climate variations using TBMs, (2) quantify the influence of extreme climate conditions on the terrestrial carbon fluxes, and (3) explore the relationships between carbon extremes and climate extremes.

## **2. Materials and Methods**

### ***2.1. Division of zones***

Our analysis was applied on each vegetated grid across the globe as well as at the regional level. To represent regional characteristics of climate impacts on ecosystems, we divided the vegetated land area into 26 regions (Figure 1) according to the IPCC SREX report on extreme events (Seneviratne et al., 2012). Such a division could benefit identification of climate extremes and how these extreme events influence regional carbon dynamics. The deficit lies in its lack of a biome standpoint, but for our objectives this division is reasonable, particularly considering the underlying mechanisms and parameterization in simulating ecosystem responses to climate variability are generally implemented in a similar way for different biomes in TBMs. Names and abbreviations of the 26 regions can be found in Figure 1. Regional climate characteristics and vegetation types are described in Table S1. In this study, high latitudes refer to land areas between 60° N and 90° N, middle latitudes refer to land areas between 30° N and 60° N and between 30° S and 60° S, and low latitudes refer to land areas from 30° N to 30° S.

### ***2.2. ISIMIP2a terrestrial biosphere models and simulation results***

The Inter-Sectoral Impact Model Intercomparison Project (ISIMIP) provides a framework to quantify climate change impacts on multiple sectors in the earth system. We used simulations of seven TBMs in ISIMIP2a (Reyer et al., 2019), including CARAIB (Dury et al., 2011), DLEM (Tian et al., 2015), LPJ-GUESS (B. Smith et al., 2001), LPJml (Bondeau et al.,

2007), ORCHIDEE (Krinner et al., 2005), VEGAS (Zeng et al., 2005), and VISIT (Ito & Inatomi, 2012). All the seven models explicitly consider the dynamics of terrestrial carbon fluxes and pools in response to environmental changes, including climate change, CO<sub>2</sub> concentration, and land cover change. But large differences exist among models in structure and representation of biophysical, biogeochemical and hydrological processes, especially in representing carbon fluxes in responding to temperature and precipitation changes. In the ISIMIP2a framework, the TBMs were driven by consistent input datasets and ran under the same simulation protocol at a spatial resolution of 0.5° latitude/longitude. Time-series of land use data were taken from the HYDE3/MIRCA2000, and the inter-annual CO<sub>2</sub> concentration was based on time series of global atmospheric CO<sub>2</sub>-concentrations data from Meinshausen, Raper & Wigley (2011) for 1765-2005 and Dlugokencky & Tans (2014) for 2006-2013. The novelty of the ISIMIP2a ensemble compared to other DGVM ensembles is that several different observation-based global climate datasets, including GSWP3 (1901-2010), PGMFD (1901-2012), and WATCH+WFDEI (1901-2010), were used to drive the TBMs. The ISIMIP2a outputs of carbon fluxes have been intensively compared and validated with multiple benchmarking datasets, including remote sensing products, data-driven products, and global residual land sink results (Cantú et al., 2018; Chang et al., 2017; Chen et al., 2017; Ito et al., 2017). The climate-data-induced uncertainty in model estimates of ecosystem productivity is substantial (Wu et al., 2017). In this study, we analyzed inter-annual model simulations driven by GSWP3, PGMFD, and WATCH+WFDEI climate datasets. As simulations of CARAIB and VEGAS models driven by PGMFD were not available, a total of 19 sets of model-simulated carbon fluxes were included in our analysis.

### ***2.3. De-trended anomalies of climate variables and carbon fluxes***

Analyses in this study were based on the de-trended anomalies of annual climate and carbon fluxes. For each grid cell, linear trends in annual temperature, precipitation, and solar

radiation were computed. Then we calculated the de-trended climate conditions by subtracting the linear trends from the original climate time series. Likewise, linear trends in inter-annual carbon fluxes were subtracted from the 19 sets of model simulations to exclude the influences of long-term climate trend and non-climatic environmental drivers, such as the increases in CO<sub>2</sub> concentration and nitrogen deposition. The de-trended anomalies of carbon fluxes were assumed to result from climate variations.

#### ***2.4. Sensitivities of inter-annual carbon fluxes to climate variations***

Climate impacts on terrestrial carbon fluxes differ over time and space under the influences of multiple environmental factors. It is necessary to understand the sensitivity of ecosystem carbon fluxes to inter-annual temperature and precipitation changes when examining the impacts of climate extremes. We calculated the apparent sensitivity of ecosystem carbon fluxes to climate variables using the Multiple Linear Regression (MLR) method (Piao et al., 2013),

$$\Delta C_{flux} = b_0 + b_1 \Delta T + b_2 \Delta P + b_3 \Delta R + \varepsilon \quad (1)$$

where  $\Delta C_{flux}$  refers to the de-trended annual anomalies of Net Primary Productivity ( $NPP$ ) ( $\text{g C m}^{-2} \text{ yr}^{-1}$ ), Heterotrophic respiration ( $Rh$ ) ( $\text{g C m}^{-2} \text{ yr}^{-1}$ ), or Net Ecosystem Productivity ( $NEP = NPP - Rh$ ) ( $\text{g C m}^{-2} \text{ yr}^{-1}$ );  $\Delta T$ ,  $\Delta P$ , and  $\Delta R$  are the de-trended annual anomalies of mean temperature ( $^{\circ}\text{C}$ ), precipitation ( $\text{mm yr}^{-1}$ ), and shortwave solar radiation ( $\text{watt m}^{-2}$ ), respectively;  $b_1$ ,  $b_2$ , and  $b_3$  are regression coefficients, representing the apparent sensitivities of carbon fluxes to temperature, precipitation, and solar radiation, respectively;  $b_0$  is the fitted intercept;  $\varepsilon$  is the residue error in the multiple linear regression. We also analyzed the spatial patterns of model consistency and divergence among the 19 simulations. It is assumed that model results show consistency in an area when over 75% of the simulations have the same sign (either positive or negative) of sensitivity.

Interactive effects of precipitation and temperature may strengthen or weaken the impacts of a single climate factor on ecosystem carbon fluxes (Luo et al., 2008). To identify the interactive precipitation-temperature effects, we added an interaction term ( $\Delta T \Delta P$ ) in the regression model.

$$\Delta C_{flux} = \gamma_0 + \gamma_1 \Delta T + \gamma_2 \Delta P + \gamma_3 \Delta T \Delta P + \varepsilon \quad (2)$$

where  $\gamma_1$  is the impact of temperature on carbon fluxes if no temperature-precipitation interaction;  $\gamma_2$  is the impact of precipitation on carbon fluxes if no temperature-precipitation interaction; and  $\gamma_3$  is the coefficient of the interactive effects of temperature and precipitation, indicating the changed temperature impacts by precipitation variation and the changed precipitation impacts by temperature variation.

### ***2.5. Identifying extreme climate and carbon flux years***

Following the definition in the IPCC SREX report (Seneviratne et al., 2012), we identified annual climate extremes through the upper and lower tails of the probability distribution of the de-trended annual temperature and precipitation in each grid. The 10<sup>th</sup> and 90<sup>th</sup> percentiles were used as the criteria for extremely cold/dry and extremely hot/wet years. It is worth noting that extreme years were not completely the same in the GSWP3, PGMFD, and WATCH+WFDEI climate datasets. Extreme carbon years (extremely high or low NPP, Rh, and NEP) were also identified using the same percentile threshold for the 19 sets of ISIMIP2a model simulations.

Then we calculated the average anomalies of carbon fluxes in the climate extreme years for each climate dataset. For example, in each grid, the extreme hot years were identified in the climate datasets, and then average NPP, Rh, and NEP anomalies were calculated in these years. Anomalies of regional and global carbon fluxes in the climate extreme years were calculated

by averaging the gridded carbon fluxes in climate extreme years. Likewise, for each grid, we identified carbon extreme years in the 19 sets of model simulations, and calculated the average anomalies of precipitation and temperature in the carbon extremes years. Regional and global climate anomalies in the carbon extreme years were also obtained by averaging the gridded climate anomalies during carbon extreme years.

We further estimated the fraction of carbon extreme years that coincide with extreme climate years (Table S2). The probability of high carbon extreme years that coincided with climate extreme years was estimated as  $[n(\text{Hcarbon\_Hclimate}) + n(\text{Hcarbon\_Lclimate})] / 40$ , where  $n(\text{Hcarbon\_Hclimate})$  is the number of years in which high carbon extremes occurred with high climate extremes, and  $n(\text{Hcarbon\_Lclimate})$  is the number of years in which high carbon extremes occurred with low climate extremes, and “40” refers to the total number of years in the model simulation period (1971 - 2010). Likewise, the probability of low carbon extreme years that coincided with climate extreme years was estimated as  $[n(\text{Lcarbon\_Hclimate}) + n(\text{Lcarbon\_Lclimate})] / 40$ .  $n(\text{Lcarbon\_Hclimate})$  is the number of years in which low carbon extremes occurred with high climate extremes, and  $n(\text{Lcarbon\_Lclimate})$  is the number of years in which low carbon extremes occurred with low climate extremes.

## **2.6. Satellite-based analysis**

We collected the global NPP data during 1982 - 2016 derived from the remote sensing imageries of the Advanced Very High Resolution Radiometer (AVHRR) (W. Smith et al., 2016). This dataset was developed based on the light use efficiency (LUE) model scaled by temperature and water stress (<https://wkolby.org/data-code/>). Temperature and water stress scalars were estimated by daily vapor pressure deficit (VPD) and minimum temperature in the

CRUNCEP v8 climate data. Using the same methodology described above, we calculated the sensitivity of this satellite-based NPP to climate variations to compare with TBM-based results.

### **3. Results**

#### ***3.1. Sensitivity of carbon fluxes to climate variations in TBMs***

##### ***3.1.1 Sensitivity of carbon fluxes to temperature***

The sensitivity of each carbon flux to temperature or precipitation showed large spatial variations (Figure 2), and differed substantially among NPP, Rh, and NEP. NPP sensitivity to temperature varied significantly along the latitudinal gradient (Figure 2A). Areas with positive and negative NPP sensitivity accounted for 43.5% and 56.5% of the total vegetated land area. NPP increased with annual temperature anomalies in the high latitudes at a rate of  $7.9 \pm 2.2$  g C m<sup>-2</sup> °C<sup>-1</sup> (avg.  $\pm$  1 std. dev, the same hereafter for model results), but decreased with temperature in the low latitudes at a rate of  $-42.9 \pm 14.3$  g C m<sup>-2</sup> °C<sup>-1</sup>. At the global level, a 1 °C increase in temperature reduced NPP by  $18.1 \pm 9.9$  g C m<sup>-2</sup> (or  $2 \pm 1.1$  Pg C; Table 1). The transition from the positive temperature response of NPP to the negative temperature response of NPP mainly located between 40 °N and 50 °N and between 40 °S and 50 °S (Figure 3). NPP showed the strongest negative sensitivity to temperature in region 24: SEA (Southeast Asia,  $-73.3 \pm 40.7$  g C m<sup>-2</sup> °C<sup>-1</sup>) and region 7: AMZ (Amazon,  $-66.2 \pm 17.8$  g C m<sup>-2</sup> °C<sup>-1</sup>; Figure S1).

At the global level, Rh showed a positive response to temperature over 87.7% of the vegetated land area, and a 1 °C increase in temperature enhanced Rh by  $11 \pm 3.5$  g C m<sup>-2</sup> yr<sup>-1</sup> ( $1.2 \pm 0.4$  Pg C). The spatial variation of Rh sensitivity to temperature was relatively small over latitudinal regions ( $9 \pm 5.1$  g C m<sup>-2</sup> °C<sup>-1</sup> in the high latitudes,  $11.8 \pm 3.6$  g C m<sup>-2</sup> °C<sup>-1</sup> in the middle latitudes, and  $10.8 \pm 6.2$  g C m<sup>-2</sup> °C<sup>-1</sup> in the low latitudes). The highest Rh sensitivity was found in region 24: SEA (Southeast Asia,  $21.5 \pm 22$  g C m<sup>-2</sup> °C<sup>-1</sup>). The only two regions

with a negative Rh sensitivity were region 17: SAF (Southern Africa,  $-1.1 \pm 10.2 \text{ g C m}^{-2} \text{ }^{\circ}\text{C}^{-1}$ ) and region 25: NAU (Northern Australia,  $-1 \pm 16.6 \text{ g C m}^{-2} \text{ }^{\circ}\text{C}^{-1}$ ).

Warming suppressed global NPP and stimulated global Rh, leading to a substantial reduction in global NEP by  $-29 \pm 10.9 \text{ Pg C m}^{-2} \text{ }^{\circ}\text{C}^{-1}$  or  $-3.2 \pm 1.2 \text{ Pg C }^{\circ}\text{C}^{-1}$  (NEP is counted positively when ecosystems gain carbon). The fraction of global vegetated land area with negative NEP sensitivity was as high as 81.1%, while the areas with positive sensitivity were restricted to the high latitudes and the Tibetan Plateau. The largest negative sensitivity occurred in the low latitudes ( $-53.4 \pm 15.2 \text{ g C m}^{-2} \text{ }^{\circ}\text{C}^{-1}$ ), particularly for region 24: ( $-93.7 \pm 42.6 \text{ g C m}^{-2} \text{ }^{\circ}\text{C}^{-1}$ ) and region 7: AMZ ( $-82.5 \pm 16.6 \text{ g C m}^{-2} \text{ }^{\circ}\text{C}^{-1}$ ). NEP in the high latitudes was less sensitive to temperature anomalies ( $-1.1 \pm 4.5 \text{ g C m}^{-2} \text{ }^{\circ}\text{C}^{-1}$ ) than that in the middle and low latitudes but still shows a negative sensitivity.

The NPP sensitivities to temperature varied along a gradient of mean annual temperature (MAT) (Figure S2). Below  $10 \text{ }^{\circ}\text{C}$ , NPP sensitivity to temperature was positive, while NPP sensitivity was negative above  $15 \text{ }^{\circ}\text{C}$ . These results are consistent with previous results based on tree rings (Bondeau et al., 2007; Klesse et al., 2018). For NEP, positive and negative sensitivities diverged at  $0 \text{ }^{\circ}\text{C}$ , with the positive response below  $0 \text{ }^{\circ}\text{C}$  and the negative response above  $0 \text{ }^{\circ}\text{C}$ . Rh sensitivity was positive over most of the MAT zones, except in some areas with high temperature ( $> 20 \text{ }^{\circ}\text{C}$ ) and moderate precipitation ( $400 \text{ mm yr}^{-1}$  to  $800 \text{ mm yr}^{-1}$ ).

The seven TBMs showed consistency in 62.5%, 69.8%, and 52.4% of the global vegetated land area for the sensitivity of NPP, Rh, and NEP (Figure 2A, B, and C), respectively. NPP and Rh had more consistent modeled sensitivity than NEP. For NPP, the major divergences occurred in the transition regions from positive sensitivity to negative sensitivity, including the Continental US, Europe, Southwest Russia, and Southeast China. For Rh, the

major divergences were in Mexico, India, Southeast Asia, and Southeast Australia. For NEP, divergences were primarily in the middle and high latitudes.

### **3.1.2. Sensitivity of carbon fluxes to precipitation**

NPP sensitivity to precipitation was positive over 95.6% of the vegetated land area (Figure 2). The middle latitudes had a greater positive NPP sensitivity to precipitation than the low and high latitudes (Figure 3 and Table 1). At the global level, a 1 mm increase in annual precipitation enhanced NPP by  $0.21 \pm 0.1 \text{ g C m}^{-2}$ . Higher NPP sensitivity was found in relatively dry area (Figure S1), for example region 26: SAU (Southern Australia and New Zealand,  $0.42 \pm 0.17 \text{ g C m}^{-2} \text{ mm}^{-1}$ ), region 17: SAF (Southern Africa,  $0.32 \pm 0.08 \text{ g C m}^{-2} \text{ mm}^{-1}$ ), and region 3: WNA (Western North America,  $0.32 \pm 0.15 \text{ g C m}^{-2} \text{ mm}^{-1}$ ).

Rh sensitivity to precipitation was found to be positive over 91.5% of the vegetated land area. On average, Rh sensitivity was  $0.07 \pm 0.04 \text{ g C m}^{-2} \text{ mm}^{-1}$ , which was about one third of NPP sensitivity. The impacts of precipitation anomalies on Rh partially offset the impacts of precipitation on NPP, resulting in a positive NEP sensitivity of  $0.14 \pm 0.12 \text{ g C m}^{-2} \text{ mm}^{-1}$ . NEP sensitivity was the highest in the middle latitudes ( $0.17 \pm 0.16 \text{ g C m}^{-2} \text{ mm}^{-1}$ ) but the lowest in the high latitudes ( $0.05 \pm 0.14 \text{ g C m}^{-2} \text{ mm}^{-1}$ ), indicating that precipitation changes could play a more important role in carbon sink anomalies in the middle-latitude ecosystems than the other regions. Similar to NPP sensitivity, the highest positive NEP sensitivity was in relatively dry regions, for example, region 26: SAU (Southern Australia and New Zealand,  $0.32 \pm 0.2 \text{ g C m}^{-2} \text{ mm}^{-1}$ ), region 16: EAF (Eastern Africa;  $0.22 \pm 0.15 \text{ g C m}^{-2} \text{ mm}^{-1}$ ), and region 3: WNA (Western North America;  $0.22 \pm 0.18 \text{ g C m}^{-2} \text{ mm}^{-1}$ ).

TBMs presented consistency in 78.3%, 51.5%, and 50.9% of the global vegetated land area for the sensitivity of NPP, Rh, and NEP (Figure 2D, E, and F), respectively. NPP has more consistent modeled sensitivity than Rh and NEP. Divergences in NPP sensitivity to

precipitation were found in the Siberia region. Rh sensitivity showed considerable differences among the TBMs primarily in the tropical regions, including Amazon forests, tropical Africa, and Southeast Asia. Divergences in NEP sensitivity resided in the boreal region, eastern US, eastern China, and Southeast Asia.

### ***3.1.3. Interactive effects of temperature and precipitation***

On global average, the correlation coefficient for the interaction term ( $\gamma_3$ ) was  $0.026 \pm 0.009 \text{ g C m}^{-2} \text{ }^\circ\text{C}^{-1} \text{ mm}^{-1}$  for NPP,  $0.017 \pm 0.010 \text{ g C m}^{-2} \text{ }^\circ\text{C}^{-1} \text{ mm}^{-1}$  for Rh, and  $0.009 \pm 0.005 \text{ g C m}^{-2} \text{ }^\circ\text{C}^{-1} \text{ mm}^{-1}$  for NEP (Figure 4). At the global level, the TBMs reached an agreement on the positive interactive effects of temperature and precipitation. The interactive effects showed considerable spatial variations. Large interactive effects on NPP mainly occurred in the hot and dry South America and Africa, such as, NEB ( $0.075 \pm 0.034 \text{ g C m}^{-2} \text{ }^\circ\text{C}^{-1} \text{ mm}^{-1}$ ), SSA ( $0.070 \pm 0.040 \text{ g C m}^{-2} \text{ }^\circ\text{C}^{-1} \text{ mm}^{-1}$ ), SAH ( $0.068 \pm 0.043 \text{ g C m}^{-2} \text{ }^\circ\text{C}^{-1} \text{ mm}^{-1}$ ), WAF ( $0.076 \pm 0.034 \text{ g C m}^{-2} \text{ }^\circ\text{C}^{-1} \text{ mm}^{-1}$ ), and SAF ( $0.082 \pm 0.045 \text{ g C m}^{-2} \text{ }^\circ\text{C}^{-1} \text{ mm}^{-1}$ ) (Figure 4). Large interactive effects on NEP also occurred in these regions ( $0.028 \pm 0.025 \text{ g C m}^{-2} \text{ }^\circ\text{C}^{-1} \text{ mm}^{-1}$  in NEB,  $0.027 \pm 0.016 \text{ g C m}^{-2} \text{ }^\circ\text{C}^{-1} \text{ mm}^{-1}$  in SSA,  $0.039 \pm 0.021 \text{ g C m}^{-2} \text{ }^\circ\text{C}^{-1} \text{ mm}^{-1}$  in SAH,  $0.034 \pm 0.021 \text{ g C m}^{-2} \text{ }^\circ\text{C}^{-1} \text{ mm}^{-1}$  in WAF, and  $0.022 \pm 0.022 \text{ g C m}^{-2} \text{ }^\circ\text{C}^{-1} \text{ mm}^{-1}$  in SAF). Additionally, models showed considerable divergences in the spatial pattern of the interactive effects. For the sign of  $\gamma_3$ , the TBMs had agreement only on 3.4%, 1.1%, and 1.4% of the global vegetated land area for NPP, Rh, and NEP, respectively.

### ***3.2. Impacts of climate extremes on annual carbon fluxes in Terrestrial Biosphere Models***

Over the global vegetated land area, the average temperature anomaly was  $-0.99 \text{ }^\circ\text{C}$  in the extremely cold years and  $0.96 \text{ }^\circ\text{C}$  in the extremely hot years during 1971-2010 (“extreme” refers to outside 10% and 90% percentiles in this study; Table 2). The magnitude of temperature anomalies in extremely cold/hot years was the largest in the high latitudes ( $-1.82/1.72 \text{ }^\circ\text{C}$ ) and

the smallest in the low latitudes ( $-0.60/0.61$  °C; Figure S3). The global average precipitation anomaly was  $-268$  mm yr<sup>-1</sup> in the extremely dry years and  $303$  mm yr<sup>-1</sup> in the extremely wet years. In contrast to extreme temperature, the magnitude of precipitation anomalies in the extremely dry/wet years was the largest in the low latitudes ( $-383.3/431.9$  mm yr<sup>-1</sup>) and the smallest in the high latitudes ( $-117.8/135.1$  mm yr<sup>-1</sup>; Figure S3).

Due to the different sensitivities of carbon fluxes to climate variables and the magnitudes of climate extremes over regions, the responses of carbon fluxes in the climate extremes showed large spatial variations. At the global scale, NPP on average had a positive anomaly of  $18 \pm 9.9$  g C m<sup>-2</sup> yr<sup>-1</sup> during the extremely cold years and a negative anomaly of  $-18.5 \pm 9.3$  g C m<sup>-2</sup> yr<sup>-1</sup> in the extremely hot years (Figure S4). Although the low latitudes generally had a smaller magnitude of temperature anomalies in the extreme years, the impacts of extreme temperature on NPP anomaly were larger than in the other latitudinal regions because of the larger (more negative) sensitivity of NPP to temperature. In the high latitudes, NPP was stimulated in the extremely hot years, but suppressed in the extremely cold years, which presented an opposite pattern to the response of global NPP to temperature extremes.

At the global scale, NPP showed negative anomalies of  $-60.9 \pm 24.4$  g C m<sup>-2</sup> yr<sup>-1</sup> in the extremely dry years and positive anomalies of  $46.7 \pm 19.5$  g C m<sup>-2</sup> yr<sup>-1</sup> in the extremely wet years (Figure S5). Hence, there is a negative asymmetry of global NPP between extremely dry and extremely wet years. The impact of precipitation extremes on NPP was about 3 times as large as the impact of temperature extremes, indicating that the TBMs simulated a stronger impact of precipitation extremes in controlling global NPP variations than that of temperature extremes. Impacts of extreme precipitation were similar to the impacts of extreme temperature in the high latitudes, while the impacts of extreme precipitation (extremely dry + extremely wet) were about 13 and 1.8 times of the impacts of extreme temperature (extremely hot + extremely cold) in the middle latitudes and low latitudes, respectively (Table 2).

The global average Rh anomaly was  $-6.9 \pm 4.9 \text{ g C m}^{-2} \text{ yr}^{-1}$  in the extremely cold years and  $7 \pm 4.6 \text{ g C m}^{-2} \text{ yr}^{-1}$  in the extremely hot years. Impacts of temperature extremes on Rh in the high latitudes ( $-15.4 \pm 8.9 \text{ g C m}^{-2} \text{ yr}^{-1}$  in the extremely cold years and  $16 \pm 8.5 \text{ g C m}^{-2} \text{ yr}^{-1}$  in the extremely hot years) were stronger than those in the other latitudinal regions but still symmetrical. The global average Rh anomaly was  $-16.5 \pm 11.4 \text{ g C m}^{-2} \text{ yr}^{-1}$  in the extremely dry years and  $13.6 \pm 10.7 \text{ g C m}^{-2} \text{ yr}^{-1}$  in the extremely wet years, which was about twice the impacts of temperature extremes. Extreme precipitation impacts on Rh were stronger in the tropical regions than the boreal regions.

At the global level, extremely hot climate conditions reduced NPP but enhanced Rh, leading to a large decline in annual NEP of  $-25.5 \pm 11.5 \text{ g C m}^{-2} \text{ yr}^{-1}$ . During the extremely dry years, NPP reduction was larger than Rh reduction, resulting in a substantial NEP decrease of  $-44.4 \pm 11.5 \text{ g C m}^{-2} \text{ yr}^{-1}$ . The impacts of precipitation extremes on the terrestrial carbon fluxes were stronger than those of temperature extremes at the global scale. Similar patterns were also found for all the three latitudinal belts (Table 2). In extreme temperature and precipitation years, NEP showed larger reductions in the low latitudes than in the high latitudes, indicating that climate extremes influenced the global carbon sink/source primarily through altering carbon fluxes in the low-latitude ecosystems.

As shown in Figure 5, impacts of precipitation extremes on NPP and NEP were stronger in climate space with high MAT ( $> 15 \text{ }^\circ\text{C}$ ) and moderate Mean Annual Precipitation (MAP) ( $400 - 1200 \text{ mm yr}^{-1}$ ), which is corresponding to the arid/semi-arid zones in temperate and tropical regions. The largest NPP reduction during the extremely hot years occurred in region 17: SAF (Southern Africa,  $-70.4 \pm 16 \text{ g C m}^{-2} \text{ yr}^{-1}$ ), region 25: NAU (northern Australia and New Zealand,  $43.6 \pm 34.4 \text{ g C m}^{-2} \text{ yr}^{-1}$ ), and region 24: SEA (Southeast Asia,  $43 \pm 21.7 \text{ g C m}^{-2} \text{ yr}^{-1}$ ) (Figure S6). The largest NPP reduction during the extremely dry years occurred in region 25: NAU (northern Australia and New Zealand,  $-131.7 \pm 35.9 \text{ g C m}^{-2} \text{ yr}^{-1}$ ), region 8: NEB

(N.E. Brazil,  $-118.7 \pm 36.7 \text{ g C m}^{-2} \text{ yr}^{-1}$ ), region 26: SAU (S. Australia/New Zealand,  $109.9 \pm 47.1 \text{ g C m}^{-2} \text{ yr}^{-1}$ ), and region 17: SAF (Southern Africa,  $109.9 \pm 24.2 \text{ g C m}^{-2} \text{ yr}^{-1}$ ). These four regions also experienced the largest NEP reduction in extremely dry years (region 25 NAU:  $-97.1 \pm 38.9 \text{ g C m}^{-2} \text{ yr}^{-1}$ , region 8 NEB:  $-90 \pm 48.6 \text{ g C m}^{-2} \text{ yr}^{-1}$ , region 26 SAU:  $-85 \pm 55 \text{ g C m}^{-2} \text{ yr}^{-1}$ , and region 17 SAF:  $-77 \pm 33.3 \text{ g C m}^{-2} \text{ yr}^{-1}$ ) and the largest NEP increase in the extremely wet years (region 25 NAU:  $94.5 \pm 42.6 \text{ g C m}^{-2} \text{ yr}^{-1}$ , region 8 NEB:  $82.6 \pm 48 \text{ g C m}^{-2} \text{ yr}^{-1}$ , region 26 SAU:  $70.5 \pm 45.2 \text{ g C m}^{-2} \text{ yr}^{-1}$ , and region 17 SAF:  $65.4 \pm 29.2 \text{ g C m}^{-2} \text{ yr}^{-1}$ ). This suggests that semi-arid ecosystems in Australia, South America, and South Africa contributed the most to the global variations of carbon fluxes in the extreme climate years in the ISIMIP models. This result was consistent with Poulter et al. (2014) and Ahlström et al. (2015), which found that the inter-annual variability of global carbon fluxes was primarily controlled by temperature and precipitation variations in the semi-arid ecosystems in the Southern Hemisphere.

### ***3.3. Carbon flux extremes and their relationships with climate in TBMs***

At the global scale, average NPP anomaly was  $-115.7 \pm 26.6 \text{ g C m}^{-2} \text{ yr}^{-1}$  in the extreme low NPP years and  $107.2 \pm 25.1 \text{ g C m}^{-2} \text{ yr}^{-1}$  in the extreme high NPP years. The average Rh anomaly was  $-50.9 \pm 10.7 \text{ g C m}^{-2} \text{ yr}^{-1}$  in the extreme low Rh years and  $54.9 \pm 20.2 \text{ g C m}^{-2} \text{ yr}^{-1}$  in the extreme high Rh years; and the average NEP anomaly was  $-112.6 \pm 39.4 \text{ g C m}^{-2} \text{ yr}^{-1}$  in the extreme low NEP years and  $103.3 \pm 34.3 \text{ g C m}^{-2} \text{ yr}^{-1}$  in the extreme high NEP years (Figure S7).

In the high latitudes, extreme high NPP years were usually associated with positive temperature anomalies. For example, the average temperature anomaly in extreme high NPP years was  $0.9 \pm 0.15 \text{ }^\circ\text{C}$  in region 2: CGI,  $0.57 \pm 0.2 \text{ }^\circ\text{C}$  in region 1: ALA, and  $0.42 \pm 0.21 \text{ }^\circ\text{C}$  in region 11: NEU. In the relatively dry regions, extreme high NPP years were associated with

positive precipitation and negative temperature anomalies (Figure 6). For example, in extreme high NPP years, average temperature and precipitation anomalies were  $-0.39 \pm 0.16$  °C and  $273.4 \pm 52.7$  mm yr<sup>-1</sup> in region 25 NAU,  $-0.21 \pm 0.06$  °C and  $260.1 \pm 84.4$  mm yr<sup>-1</sup> in region 8 NEB, and  $-0.27 \pm 0.07$  °C and  $174.4 \pm 46$  mm yr<sup>-1</sup> in region 17 SAF.

At the regional level, extreme high Rh years coincided with positive precipitation anomalies over all the 26 regions and positive temperature anomalies over 24 regions (Figure 6). The two regions with negative temperature anomalies were region 25: NAU and region 17: SAF. In extreme high NEP years, 19 regions showed negative temperature and positive precipitation anomalies (Figure 6).

The spatial distribution of the fraction of carbon extremes years that coincided with climate extreme years shows that, over most of the global vegetated land area, NPP and NEP extreme years did not occur in extreme temperature years (Figure 7a, c, i, k). In the semi-arid regions of the middle and low latitudes, low NPP and NEP extreme years more frequently occurred during precipitation extreme years (Figure 7d, l). In Eastern Canada and Central Europe, we found a higher fraction of Rh extreme years that coincided with climate extreme years (extreme high temperature; Figure 7e, g). It is also worth noting that a large fraction of carbon extremes over the vegetated land area did not occur during climate extreme years.

### ***3.4. Comparison between model-based sensitivity and satellite-based sensitivity***

Sensitivity of satellite-based NPP to temperature was negative in the low latitudes and positive in the high latitudes (Figure 8A). The transition occurred in the middle-latitudes. This pattern was consistent with that of the model-based results (Figure 2). These results partly reflect the different climate factors in controlling vegetation growth across climate zones, i.e. temperature and growing season length in high latitudes, and moisture and radiation in the low latitudes (Lucht et al., 2002; Nemani et al., 2003). The model-based NPP sensitivity to

temperature had the same sign as the satellite-based NPP sensitivity in 85.3% of the global vegetated area. The curves of the cumulative vegetated land area against sensitivity suggest that the model-based NPP sensitivity to temperature is generally consistent with the satellite-based results. However, the model-based NPP sensitivity to precipitation showed significant differences with the satellite-based results. Although the same sign of NPP sensitivity to precipitation between model results and satellite results existed in 76.9% of the global vegetated area, the TBMs simulated a larger NPP sensitivity than satellite estimates in 91.2% of the global vegetated area. On global average, the satellite-based NPP sensitivity to precipitation was  $0.04 \text{ g C m}^{-2} \text{ mm}^{-1}$ , comparing to the model-ensemble-mean of  $0.21 \text{ g C m}^{-2} \text{ mm}^{-1}$ .

#### **4. Discussion**

The results strongly suggest that extremely dry events inhibited both global NPP and Rh simulated by TBMs. Impact of extremely dry events on NPP was 3.7 times that of Rh, leading to a large reduction of the carbon sink (i.e., NEP) in the extremely dry years. The different responses of NPP and Rh to droughts in the TBMs were consistent with previous reports based on site-level data synthesis (Shi et al., 2014) and global level analysis (Schwalm et al., 2010; Pan et al. 2015). Spatially, impacts of extreme droughts on the terrestrial carbon fluxes were stronger in tropical and temperate regions, especially semi-arid Africa, South America, and Australia. These regions were also more sensitive to extremely wet events than other areas and, therefore, played more important roles in affecting the inter-annual variations of the global terrestrial carbon sink (Ahlström et al., 2015; Poulter et al., 2014).

Extremely high temperature reduced global NPP and enhanced global ecosystem Rh, leading to a reduction in the terrestrial carbon sink. NPP anomalies showed a reduction during extremely dry events and extremely hot events, but Rh increased under both conditions. The

reduced NEP in extremely hot years was caused by the concurrent impacts on NPP and Rh, while the reduced NEP in extremely dry years was due to the larger reduction in NPP than Rh. Notably, we found that, in the TBMs, extreme carbon years did not necessarily coincide with extreme temperature or precipitation years over a large fraction of the global vegetated land, though climate extremes significantly affected the anomalies of terrestrial carbon fluxes. The compound effects of concurrent temperature and precipitation anomalies that are not extreme climate events could be the major reason for the decoupling between carbon and climate extremes. The interactions between temperature variations and precipitation deficits could substantially alter terrestrial carbon dynamics, for example, the combined dry and hot extreme in Europe 2003 (Ciais et al., 2005) and the combined dry and hot extreme in California 2014 (AghaKouchak et al., 2014). However, extreme temperature and precipitation events did not always occur simultaneously. Thus, regional carbon extremes occurred in the years with a specific combination of temperature and precipitation anomalies that would enhance each other's effects on carbon fluxes. For example, the extreme low NEP in AMZ was associated with high temperature (75.6 percentile) and low precipitation (26.8 percentile) but none of the temperature or precipitation anomalies was an extreme event.

The positive interactive effects of temperature and precipitation on NPP and NEP, particularly in South America and Africa, have contributed to the carbon extremes. The temperature or precipitation effect on ecosystem carbon fluxes partly depends on changes of each other. For example, the negative impacts of hot events on vegetation productivity and carbon sequestration can be strengthened by the reduced precipitation. This positive interaction is expected because the decreased precipitation could reduce soil moisture and enhance the responses of arid/semi-arid ecosystem processes to hot events (Gerten et al., 2008; Luo et al., 2008). Similarly, the negative drought impacts on ecosystem productivity can be enhanced by hot events because the high temperature could lead to more evapotranspiration, decrease soil

water availability, and then enhance vegetation sensitivity to precipitation. The concurrency of temperature and precipitation extremes could lead to devastating ecological consequences through both the additive and interactive effects of climate factors.

This study found that the most significant model discrepancies exist in the transition regions between positive sensitivity and negative sensitivity. For example, the middle latitudes have the largest model discrepancies for NPP sensitivity to temperature. In this region, leaf unfolding and vegetation growth need a certain amount of heat (Piao et al., 2015), while hot events would suppress vegetation growth (Ciais et al., 2005). Across all the TBMs, temperature effects are implicitly or explicitly considered in estimating leaf physiological activities, canopy dynamics, and carbon allocation. However, models differ largely in the parameterization of both temperature scalars and the critical thresholds for leaf onset or senescence. For example, DLEM uses a quadratic function to describe temperature effect on stomatal conductance, of which the value of optimal temperature is critical, whereas in ORCHIDEE stomatal conductance is an analytical solution of the coupled assimilation-stomatal conductance equations. A better parameterization of temperature impacts on vegetation phenology and vegetation growth could help to reduce model uncertainties.

The comparison between TBM simulations and satellite-based measurements showed that the TBMs simulated a larger sensitivity of ecosystem productivity to precipitation, particularly in tropical areas, which further lead to a larger responses of carbon sequestration during and after droughts (Beer et al., 2010). The disagreement between TBM simulations and satellite measurements could be either from the simplified representation of water stress in the LUE model or the oversensitive water impacts in the TBMs. Water stress on ecosystem productivity in the satellite observations was estimated based on the atmospheric water demand (i.e., VPD) but not water supply (i.e., soil water availability) (W. Smith et al., 2016), while the TBMs in this study included more sophisticated mechanisms to represent soil water stresses by

considering water supply and demand (e.g. Ito & Inatomi, 2012; Krinner et al., 2005; Zeng et al., 2005). Previous studies have identified the lack of dynamic root growth, hydrological redistribution, groundwater movement and reasonable carbon allocation during droughts in models are potential causes responsible for larger estimation of vegetation response to water deficit (Hu et al., 2018; Li et al., 2012; Paschalis et al., 2020). For example, during Amazon droughts, trees can increase water use efficiency and uptake water from aquifer through deep roots to mitigate drought impacts (Goll et al., 2018; Yang et al., 2018). Thus, vegetation adaption strategies and more sophisticated hydrological processes need to be taken into consideration by TBMs to improve the simulation accuracy of the changed carbon flux during drought events.

Climate controls on heterotrophic respiration were explicitly parameterized in the TBMs through the classic “first-order” decay algorithm (Parton et al., 1987). The parameterization of soil thermal conductivity and soil moisture could affect decomposition of soil organic carbon pools, as well as the forms of soil temperature and moisture scalars for  $R_h$ . However, the representations of soil temperature and moisture effects on the decay constant ( $k$ ) vary in these models, leading to the low agreement in  $R_h$  sensitivity. A comparison with the observed soil temperature and moisture effects in various vegetation types could help to improve model accuracy in simulating  $R_h$  (Riutta et al., 2012). Spatial pattern of the interactive temperature and precipitation effects showed large divergences among the simulations (Figure 4). The interaction between temperature and precipitation is a complex and non-linear process involving various regulatory mechanisms and factors, such as evapotranspiration, soil moisture, stomatal conductance, and nutrient availability, etc. However, the interactive effects on ecosystems have not been well understood (Luo et al., 2008). Therefore, in-situ Climate Extreme Experiment (Knapp et al., 2017; Smith, 2011) that manipulate temperature and precipitation simultaneously could be of particular importance to evaluate the effects of

compound climate extremes and the interactive effects of climate factors. Moreover, these data-model experiments could identify the processes or parameters in TBMs that are the key for accurately simulating responses of carbon fluxes to temperature or precipitation changes, which however are obviously out of the scope of this study.

Our results confirmed that semi-arid ecosystems in the Southern Hemisphere were particularly sensitive to precipitation extremes and made the largest contribution to the inter-annual variation of global carbon fluxes (Ahlström et al., 2015). More future research is needed to identify the changes in carbon pools and vegetation composition in semi-arid ecosystems caused by climate extremes. Moreover, our analysis emphasized the compound influences of concurrent temperature and precipitation anomalies on terrestrial carbon fluxes. These findings could be important in informing field scientists to design a series of ecological experiments in examining the responses of grassland and forests to climate extremes (Knapp et al., 2017; Wilcox et al., 2017).

Consistent with previous analysis based on TBMs from the Multi-scale Synthesis and Terrestrial Model Intercomparison Project (MsTMIP) (Zscheischler et al., 2014a), this study reveals a general pattern of climate extreme impacts on carbon fluxes. (1) Droughts tend to reduce ecosystem productivity at a larger extent and reduce terrestrial respiration at a smaller extent, and (2) heat extremes tends to reduce ecosystem productivity but enhance terrestrial respiration. By analyzing MsTMIP results, Zscheischler et al. (2014a) found that the TBM discrepancies are larger for the impacts of climate extremes on net carbon exchange than those on primary productivity and respiration. In this study, we further found that model discrepancies in the precipitation impacts are in the same magnitude for net carbon exchange and heterotrophic respiration. Additionally, this study shows the spatial distribution of model discrepancies (Figure 2) and suggests that the largest model spread occurs in the transition areas from positive sensitivity to negative sensitivity. Based on the coupled climate-carbon

cycle simulations, Zscheischler et al. (2014c) found that negative GPP and NEP extremes are driven by the concurrent heats and droughts, which is consistent with our result that carbon extremes are associated with the individual and compound influences of temperature and precipitation anomalies.

The SREX regions used in this study were first developed in the IPCC special report for climate models (Seneviratne et al 2012). It has been used to investigate the impacts of climate change as well as climate extremes. Nevertheless, for future work, it could be of interest to investigate the impacts of climate extremes based on ecoregions (Olson et al., 2001) to better account for biome dependence of climate extremes.

## **5. Conclusions**

This study investigated the influences of climate extremes on the terrestrial carbon fluxes between 1971 and 2010 using seven Terrestrial Biosphere Models (TBMs). Simulated results showed that global carbon uptake was reduced substantially during extremely dry years and extremely hot years. Hot extremes suppressed carbon sequestration through reducing carbon assimilation by photosynthesis and enhancing respiration carbon release, while dry extremes reduced carbon sequestration through causing a large decline in ecosystem carbon uptake. Ecosystems in the semi-arid region were more sensitive to climate extremes and made a larger contribution to the inter-annual variations of the global carbon fluxes. TBM simulations also suggest that a certain combination of concurrent temperature and precipitation anomalies could be more important in influencing terrestrial ecosystem carbon fluxes than the impacts of individual extreme event. The individual and interactive effects of temperature and precipitation anomalies caused carbon extremes. The interactive effects on vegetation productivity are particularly important in the hot and dry regions. TBMs simulated a stronger impacts of precipitation extremes than the satellite-derived carbon fluxes. To accurately assess the impacts of climate extremes on terrestrial carbon dynamics, it is essential to improve model

representation of complex interaction and adaptation mechanisms that are responsible for emergent properties such as ecosystem vulnerability and resilience.

### **Acknowledgements**

This study has been partially supported by National Key R & D Program of China (2017YFA0604702, 2018YFA0606001); US National Science Foundation (1903722, 1210360, 1243232); the Japan Society for Promotion of Science (17H01867). The Inter-Sectoral Impact Model Intercomparison Project Phase 2a and 2b (ISIMIP2a and ISIMIP2b) was funded by the German Federal Ministry of Education and Research (BMBF, grant no. 01LS1201A1 and 01LS1201A2). The authors declare no conflict of interest.

### **Data Availability**

The ISIMIP2a biome outputs are based on simulations of multiple global vegetation models following the ISIMIP2a protocol. The climate data and model-simulated carbon fluxes from the ISIMIP2a project can be obtained from ESGF server (<http://dataservices.gfz-potsdam.de/pik/showshort.php?id=escidoc:3997888>) (Reyer et al, 2019). The satellite-based NPP products for comparison can be downloaded from William Smith's website (<https://wkolby.org/data-code/>) (Smith et al. 2016). The code that support this analysis is archived in International Center for Climate and Global Change Research at Auburn University (<https://wp.auburn.edu/cgc/>).

## References

- AghaKouchak, A., Cheng, L., Mazdidasni, O., & Farahmand, A. (2014). Global warming and changes in risk of concurrent climate extremes: Insights from the 2014 California drought. *Geophysical Research Letters*, *41*(24), 8847–8852.
- Ahlström, A., Raupach, M. R., Schurgers, G., Smith, B., Arneeth, A., Jung, M., et al. (2015). The dominant role of semi-arid ecosystems in the trend and variability of the land CO<sub>2</sub> sink. *Science*, *348*(6237), 895–899.
- Beer, C., Reichstein, M., Tomelleri, E., Ciais, P., Jung, M., Carvalhais, N., et al. (2010). Terrestrial gross carbon dioxide uptake: global distribution and covariation with climate. *Science*, 1184984.
- Bondeau, A., Smith, P. C., Zaehle, S., Schaphoff, S., Lucht, W., Cramer, W., et al. (2007). Modelling the role of agriculture for the 20th century global terrestrial carbon balance. *Global Change Biology*, *13*(3), 679–706.
- Cantú, A. G., Frieler, K., Reyer, C. P. O., Ciais, P., Chang, J., Ito, A., et al. (2018). Evaluating changes of biomass in global vegetation models: the role of turnover fluctuations and ENSO events. *Environmental Research Letters*, *13*(7), 075002. <https://doi.org/10.1088/1748-9326/aac63c>
- Chang, J., Ciais, P., Wang, X., Piao, S., Asrar, G., Betts, R., et al. (2017). Benchmarking carbon fluxes of the ISIMIP2a biome models. *Environmental Research Letters*, *12*(4), 045002.
- Chen, M., Rafique, R., Asrar, G. R., Bond-Lamberty, B., Ciais, P., Zhao, F., et al. (2017). Regional contribution to variability and trends of global gross primary productivity. *Environmental Research Letters*, *12*(10), 105005.

Ciais, P., Reichstein, M., Viovy, N., Granier, A., Ogée, J., Allard, V., et al. (2005). Europe-wide reduction in primary productivity caused by the heat and drought in 2003.

*Nature*, 437(7058), 529.

Ciais, P., Sabine, C., Bala, G., Bopp, L., Brovkin, V., Canadell, J., et al. (2014). Carbon and other biogeochemical cycles. In *Climate change 2013: the physical science basis*.

*Contribution of Working Group I to the Fifth Assessment Report of the*

*Intergovernmental Panel on Climate Change* (pp. 465–570). Cambridge University Press.

Dlugokencky, E., & Tans, P. (2014). *Trends in atmospheric carbon dioxide, National*

*Oceanic & Atmospheric Administration, Earth System Research Laboratory*

(NOAA/ESRL).

Dury, M., Hambuckers, A., Warnant, P., Henrot, A., Favre, E., Ouberdous, M., & François,

L. (2011). Responses of European forest ecosystems to 21 (st) century climate:

assessing changes in interannual variability and fire intensity. *IForest: Biogeosciences and Forestry*, 4, 82–99.

Frank, D., Reichstein, M., Bahn, M., Thonicke, K., Frank, D., Mahecha, M. D., et al. (2015).

Effects of climate extremes on the terrestrial carbon cycle: concepts, processes and potential future impacts. *Global Change Biology*, 21(8), 2861–2880.

Gerten, D., Luo, Y., Le Maire, G., Parton, W. J., Keough, C., Weng, E., et al. (2008).

Modelled effects of precipitation on ecosystem carbon and water dynamics in different climatic zones. *Global Change Biology*, 14(10), 2365–2379.

Goll, D. S., Joetzjer, E., Huang, M., & Ciais, P. (2018). Low phosphorus availability

decreases susceptibility of tropical primary productivity to droughts. *Geophysical Research Letters*, 45(16), 8231–8240.

Hu, Z., Shi, H., Cheng, K., Wang, Y.-P., Piao, S., Li, Y., et al. (2018). Joint structural and physiological control on the interannual variation in productivity in a temperate grassland: A data-model comparison. *Global Change Biology*, 24(7), 2965–2979. <https://doi.org/10.1111/gcb.14274>

Ito, A., & Inatomi, M. (2012). Water-use efficiency of the terrestrial biosphere: a model analysis focusing on interactions between the global carbon and water cycles. *Journal of Hydrometeorology*, 13(2), 681–694.

Ito, A., Nishina, K., Reyer, C. P., François, L., Henrot, A.-J., Munhoven, G., et al. (2017). Photosynthetic productivity and its efficiencies in ISIMIP2a biome models: benchmarking for impact assessment studies. *Environmental Research Letters*, 12(8), 085001.

Jung, M., Reichstein, M., Schwalm, C. R., Huntingford, C., Sitch, S., Ahlström, A., et al. (2017). Compensatory water effects link yearly global land CO<sub>2</sub> sink changes to temperature. *Nature*, 541(7638), 516.

Klesse, S., Babst, F., Lienert, S., Spahni, R., Joos, F., Bouriaud, O., et al. (2018). A combined tree ring and vegetation model assessment of European forest growth sensitivity to interannual climate variability. *Global Biogeochemical Cycles*, 32(8), 1226–1240.

Knapp, A. K., & Smith, M. D. (2001). Variation among biomes in temporal dynamics of aboveground primary production. *Science*, 291(5503), 481–484.

Knapp, A. K., Avolio, M. L., Beier, C., Carroll, C. J., Collins, S. L., Dukes, J. S., et al. (2017). Pushing precipitation to the extremes in distributed experiments: recommendations for simulating wet and dry years. *Global Change Biology*, 23(5), 1774–1782.

Krinner, G., Viovy, N., de Noblet - Ducoudré, N., Ogée, J., Polcher, J., Friedlingstein, P., et al. (2005). A dynamic global vegetation model for studies of the coupled atmosphere - biosphere system. *Global Biogeochemical Cycles*, 19(1).

Le Quéré, C., Andrew, R. M., Friedlingstein, P., Sitch, S., Hauck, J., Pongratz, J., et al. (2018). Global carbon budget 2018. *Earth System Science Data*, 10, 2141–2194.

Li, L., Wang, Y.-P., Yu, Q., Pak, B., Eamus, D., Yan, J., et al. (2012). Improving the responses of the Australian community land surface model (CABLE) to seasonal drought. *Journal of Geophysical Research: Biogeosciences*, 117(G4).  
<https://doi.org/10.1029/2012JG002038>

Lucht, W., Prentice, I. C., Myneni, R. B., Sitch, S., Friedlingstein, P., Cramer, W., et al. (2002). Climatic control of the high-latitude vegetation greening trend and Pinatubo effect. *Science*, 296(5573), 1687–1689.

Luo, Y., Gerten, D., Le Maire, G., Parton, W. J., Weng, E., Zhou, X., et al. (2008). Modeled interactive effects of precipitation, temperature, and [CO<sub>2</sub>] on ecosystem carbon and water dynamics in different climatic zones. *Global Change Biology*, 14(9), 1986–1999.

Meinshausen, M., Raper, S. C., & Wigley, T. M. (2011). Emulating coupled atmosphere-ocean and carbon cycle models with a simpler model, MAGICC6–Part 1: Model description and calibration. *Atmospheric Chemistry and Physics*, 11(4), 1417–1456.

Nemani, R. R., Keeling, C. D., Hashimoto, H., Jolly, W. M., Piper, S. C., Tucker, C. J., et al. (2003). Climate-Driven Increases in Global Terrestrial Net Primary Production from 1982 to 1999. *Science*, 300(5625), 1560–1563.  
<https://doi.org/10.1126/science.1082750>

Olson, D. M., Dinerstein, E., Wikramanayake, E. D., Burgess, N. D., Powell, G. V. N., Underwood, E. C., et al. (2001). Terrestrial Ecoregions of the World: A New Map of

Life on Earth A new global map of terrestrial ecoregions provides an innovative tool for conserving biodiversity. *BioScience*, 51(11), 933–938.

[https://doi.org/10.1641/0006-3568\(2001\)051\[0933:TEOTWA\]2.0.CO;2](https://doi.org/10.1641/0006-3568(2001)051[0933:TEOTWA]2.0.CO;2)

Parton, W. J., Schimel, D. S., Cole, C. V., & Ojima, D. S. (1987). Analysis of factors controlling soil organic matter levels in Great Plains Grasslands 1. *Soil Science Society of America Journal*, 51(5), 1173–1179.

Paschalis, A., Faticchi, S., Zscheischler, J., Ciais, P., Bahn, M., Boysen, L., et al. (2020). Rainfall-manipulation experiments as simulated by terrestrial biosphere models: where do we stand? *Global Change Biology*, n/a(n/a).

<https://doi.org/10.1111/gcb.15024>

Piao, S., Sitch, S., Ciais, P., Friedlingstein, P., Peylin, P., Wang, X., et al. (2013). Evaluation of terrestrial carbon cycle models for their response to climate variability and to CO<sub>2</sub> trends. *Global Change Biology*, 19(7), 2117–2132.

Piao, S., Tan, J., Chen, A., Fu, Y. H., Ciais, P., Liu, Q., et al. (2015). Leaf onset in the northern hemisphere triggered by daytime temperature. *Nature Communications*, 6(1), 1–8.

Potter, C., Klooster, S., Hiatt, C., Genovese, V., & Castilla-Rubio, J. C. (2011). Changes in the carbon cycle of Amazon ecosystems during the 2010 drought. *Environmental Research Letters*, 6(3), 034024.

Poulter, B., Frank, D., Ciais, P., Myneni, R. B., Andela, N., Bi, J., et al. (2014). Contribution of semi-arid ecosystems to interannual variability of the global carbon cycle. *Nature*, 509(7502), 600.

Reichstein, M., Bahn, M., Ciais, P., Frank, D., Mahecha, M. D., Seneviratne, S. I., et al. (2013). Climate extremes and the carbon cycle. *Nature*, 500(7462), 287.

Reyer, G Asrar, R Betts, J Chang, M Chen, P Ciais, et al. (2019). ISIMIP2a Simulation Data from Biomes Sector (V. 1.1) [Data set]. GFZ Data Services. Retrieved from <https://doi.org/10.5880/pik.2019.005>

Reyer, C. P. O., Leuzinger, S., Rammig, A., Wolf, A., Bartholomeus, R. P., Bonfante, A., et al. (2013). A plant's perspective of extremes: terrestrial plant responses to changing climatic variability. *Global Change Biology*, *19*(1), 75–89. <https://doi.org/10.1111/gcb.12023>

Riutta, T., Slade, E. M., Bebber, D. P., Taylor, M. E., Malhi, Y., Riordan, P., et al. (2012). Experimental evidence for the interacting effects of forest edge, moisture and soil macrofauna on leaf litter decomposition. *Soil Biology and Biochemistry*, *49*, 124–131.

Saleska, S. R., Didan, K., Huete, A. R., & Da Rocha, H. R. (2007). Amazon forests green-up during 2005 drought. *Science*, *318*(5850), 612–612.

Schwalm, C. R., Williams, C. A., Schaefer, K., Arneth, A., Bonal, D., Buchmann, N., et al. (2010). Assimilation exceeds respiration sensitivity to drought: A FLUXNET synthesis. *Global Change Biology*, *16*(2), 657–670.

Schwalm, C. R., Williams, C. A., Schaefer, K., Baldocchi, D., Black, T. A., Goldstein, A. H., et al. (2012). Reduction in carbon uptake during turn of the century drought in western North America. *Nature Geoscience*, *5*(8), 551.

Schwalm, C. R., Anderegg, W. R. L., Michalak, A. M., Fisher, J. B., Biondi, F., Koch, G., et al. (2017). Global patterns of drought recovery. *Nature*, *548*(7666), 202–205. <https://doi.org/10.1038/nature23021>

Seneviratne, S. I., Nicholls, N., Easterling, D., Goodess, C. M., Kanae, S., Kossin, J., et al. (2012). Changes in climate extremes and their impacts on the natural physical environment.

Shi, Z., Thomey, M. L., Mowll, W., Litvak, M., Brunsell, N. A., Collins, S. L., et al. (2014).

Differential effects of extreme drought on production and respiration: synthesis and modeling analysis. *Biogeosciences*, *11*(3), 621–633.

Smith, B., Prentice, I. C., & Sykes, M. T. (2001). Representation of vegetation dynamics in the modelling of terrestrial ecosystems: comparing two contrasting approaches within European climate space. *Global Ecology and Biogeography*, *10*(6), 621–637.

Smith, M. D. (2011). An ecological perspective on extreme climatic events: a synthetic definition and framework to guide future research. *Journal of Ecology*, *99*(3), 656–663.

Smith, W., Reed, S. C., Cleveland, C. C., Ballantyne, A. P., Anderegg, W. R. L., Wieder, W. R., et al. (2016). Large divergence of satellite and Earth system model estimates of global terrestrial CO<sub>2</sub> fertilization. *Nature Climate Change*, *6*(3), 306–310.

<https://doi.org/10.1038/nclimate2879>

Tian, H., Chen, G., Lu, C., Xu, X., Hayes, D. J., Ren, W., et al. (2015). North American terrestrial CO<sub>2</sub> uptake largely offset by CH<sub>4</sub> and N<sub>2</sub>O emissions: toward a full accounting of the greenhouse gas budget. *Climatic Change*, *129*(3–4), 413–426.

Vicente-Serrano, S. M., Gouveia, C., Camarero, J. J., Beguería, S., Trigo, R., López-Moreno, J. I., et al. (2013). Response of vegetation to drought time-scales across global land biomes. *Proceedings of the National Academy of Sciences*, *110*(1), 52–57.

Wilcox, K. R., Shi, Z., Gherardi, L. A., Lemoine, N. P., Koerner, S. E., Hoover, D. L., et al. (2017). Asymmetric responses of primary productivity to precipitation extremes: a synthesis of grassland precipitation manipulation experiments. *Global Change Biology*, *23*(10), 4376–4385.

Accepted Article  
Wu, D., Ciais, P., Viovy, N., Knapp, A. K., Wilcox, K., Bahn, M., et al. (2018). Asymmetric responses of primary productivity to altered precipitation simulated by ecosystem models across three long-term grassland sites.

Wu, Z., Ahlström, A., Smith, B., Ardö, J., Eklundh, L., Fensholt, R., & Lehsten, V. (2017). Climate data induced uncertainty in model-based estimations of terrestrial primary productivity. *Environmental Research Letters*, *12*(6), 064013.  
<https://doi.org/10.1088/1748-9326/aa6fd8>

Yang, J., Tian, H., Pan, S., Chen, G., Zhang, B., & Dangal, S. (2018). Amazon drought and forest response: Largely reduced forest photosynthesis but slightly increased canopy greenness during the extreme drought of 2015/2016. *Global Change Biology*, *24*(5), 1919–1934.

Zeng, N., Mariotti, A., & Wetzel, P. (2005). Terrestrial mechanisms of interannual CO<sub>2</sub> variability. *Global Biogeochemical Cycles*, *19*(1).

Zscheischler, J., Reichstein, M., von Buttler, J., Mu, M., Randerson, J. T., & Mahecha, M. D. (2014). Carbon cycle extremes during the 21st century in CMIP5 models: Future evolution and attribution to climatic drivers. *Geophysical Research Letters*, *41*(24), 8853–8861.

Zscheischler, J., Reichstein, M., Harmeling, S., Rammig, A., Tomelleri, E., & Mahecha, M. D. (2014). Extreme events in gross primary production: a characterization across continents. *Biogeosciences*, *11*(11), 2909–2924.

Zscheischler, J., Michalak, A. M., Schwalm, C., Mahecha, M. D., Huntzinger, D. N., Reichstein, M., et al. (2014). Impact of large - scale climate extremes on biospheric carbon fluxes: An intercomparison based on MsTMIP data. *Global Biogeochemical Cycles*, *28*(6), 585–600.

**Table 1.** Sensitivity of annual carbon fluxes to temperature and precipitation (mean  $\pm$  1 SD).

	Sensitivity to temperature (g C / m <sup>2</sup> / °C)			Sensitivity to precipitation (g C / m <sup>2</sup> / mm)		
	NPP	Rh	NEP	NPP	Rh	NEP
Global	-18.1 $\pm$ 9.9	11 $\pm$ 3.5	-29 $\pm$ 10.9	0.21 $\pm$ 0.1	0.07 $\pm$ 0.04	0.14 $\pm$ 0.12
High latitudes	7.9 $\pm$ 2.2	9 $\pm$ 5.1	-1.1 $\pm$ 4.5	0.12 $\pm$ 0.17	0.07 $\pm$ 0.06	0.05 $\pm$ 0.14
Middle latitudes	1.8 $\pm$ 10.4	11.8 $\pm$ 3.6	-9.9 $\pm$ 11.2	0.25 $\pm$ 0.14	0.08 $\pm$ 0.05	0.17 $\pm$ 0.16
Low latitudes	-42.9 $\pm$ 14.3	10.8 $\pm$ 6.2	-53.4 $\pm$ 15.2	0.2 $\pm$ 0.07	0.06 $\pm$ 0.04	0.14 $\pm$ 0.09

**Table 2.** Climate and carbon fluxes anomalies during the extreme climate years.

	Global	High-latitude	Mid-latitude	Low-latitude
Temperature anomaly (°C)				
extremely cold	-0.99	-1.81	-1.19	-0.6
extremely hot	0.96	1.72	1.13	0.61
Precipitation anomaly (mm yr <sup>-1</sup> )				
extremely dry	-268	-118	-183	-383
extremely wet	303	135	208	432
NPP anomaly (g C m <sup>-2</sup> yr <sup>-1</sup> )				
extremely cold	18 ± 9.9	-15.6 ± 4.3	3.3 ± 13.9	39.9 ± 11.6
extremely hot	-18.5 ± 9.3	12.2 ± 3.5	-3.7 ± 13.7	-39.9 ± 10.1
extremely dry	-60.9 ± 24.4	-16.7 ± 19.5	-50.3 ± 29.8	-81.9 ± 27.6
extremely wet	46.7 ± 19.5	11.9 ± 15.4	39.7 ± 23.3	62 ± 23
Rh anomaly (g C m <sup>-2</sup> yr <sup>-1</sup> )				
extremely cold	-6.9 ± 4.9	-15.4 ± 8.9	-11 ± 5.5	-1.1 ± 5.2
extremely hot	7 ± 4.6	16 ± 8.5	10.9 ± 5.7	1.2 ± 5.3
extremely dry	-16.5 ± 11.4	-11.1 ± 5.5	-15.1 ± 10.7	-19.1 ± 17.5
extremely wet	13.6 ± 10.7	9.5 ± 6.6	12.9 ± 10.4	15.3 ± 15.2
NEP anomaly (g C m <sup>-2</sup> yr <sup>-1</sup> )				
extremely cold	24.9 ± 12.4	-0.2 ± 7.4	14.3 ± 15.7	41 ± 12.8
extremely hot	-25.5 ± 11.5	-3.8 ± 7	-14.5 ± 15.6	-41.1 ± 11
extremely dry	-44.4 ± 33	-5.6 ± 15.6	-35.3 ± 36	-62.8 ± 37.7
extremely wet	33.1 ± 26	2.5 ± 12.1	26.8 ± 28.8	46.7 ± 29.3

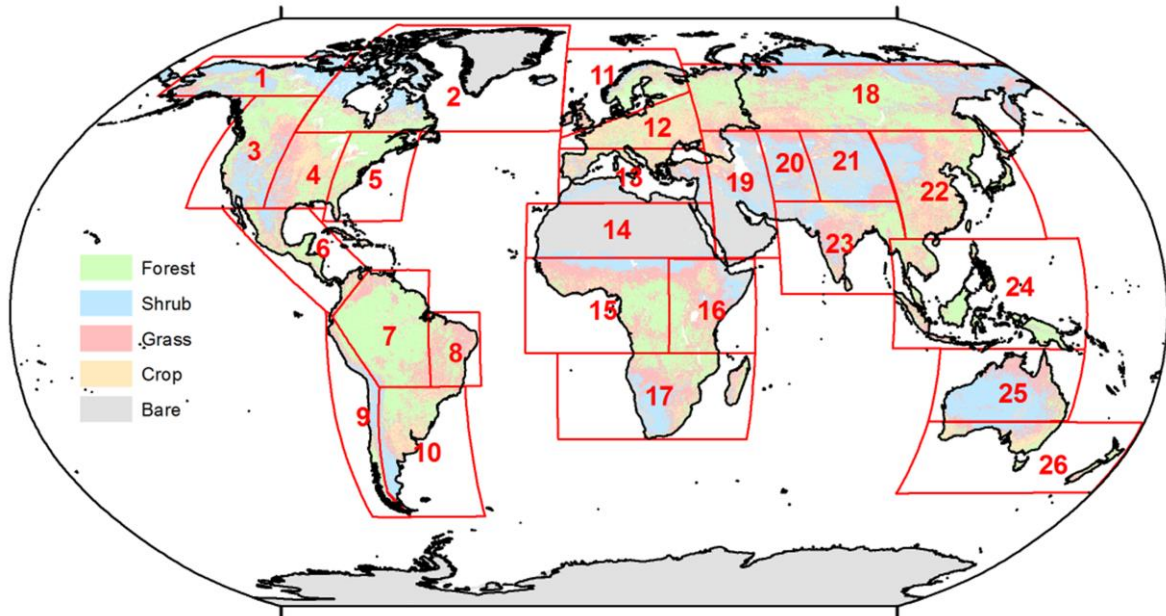


**Figure 1.** Divisions of 26 regions and the distribution of vegetation types. 1. ALA: Alaska/N.W. Canada, 2. CGI: E. Canada/Greenland/Iceland, 3. WNA: W. North America, 4. CNA: Central North America, 5. ENA: E. North America, 6. CAM: Central America and Mexico, 7. AMZ: Amazon, 8. NEB: N.E. Brazil, 9. WSA: W. Coast South America, 10. SSA: S.E. South America, 11. NEU: N. Europe, 12. CEU: Central Europe, 13. MED: S. Europe and Mediterranean, 14. SAH: Sahara, 15. WAF: W. Africa, 16. EAF: E. Africa, 17. SAF: S. Africa, 18. NAS: N. Asia, 19. WAS: W. Asia, 20. CAS: Central Asia, 21. TIB: Tibetan Plateau, 22. EAS: E. Asia, 23. SAS: S. Asia, 24. SEA: S.E. Asia, 25. NAU: N. Australia, 26. SAU: S. Australia/New Zealand. The vegetation type distribution data were from the AVHRR global land cover products (<http://glcf.umd.edu/data/landcover/data.shtml>).

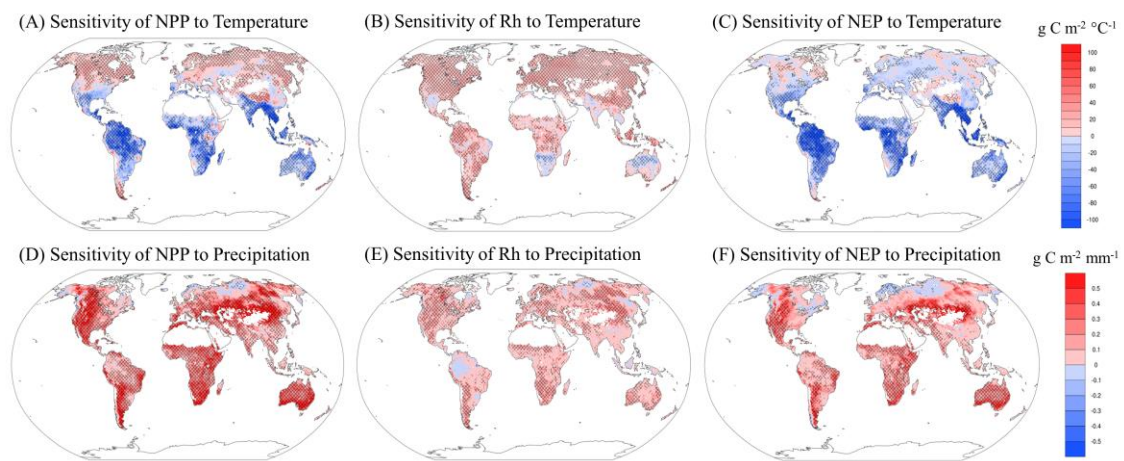


**Figure 2.** Sensitivity of terrestrial carbon fluxes (A and D: NPP, B and E: Rh, C and F: NEP) to temperature anomaly (A-C) and precipitation anomaly (D-F). Note: Maps show the averaged results of the 19 simulations. Stippling indicates locations where over 75% of the simulations have the same sign (positive or negative) of sensitivity.

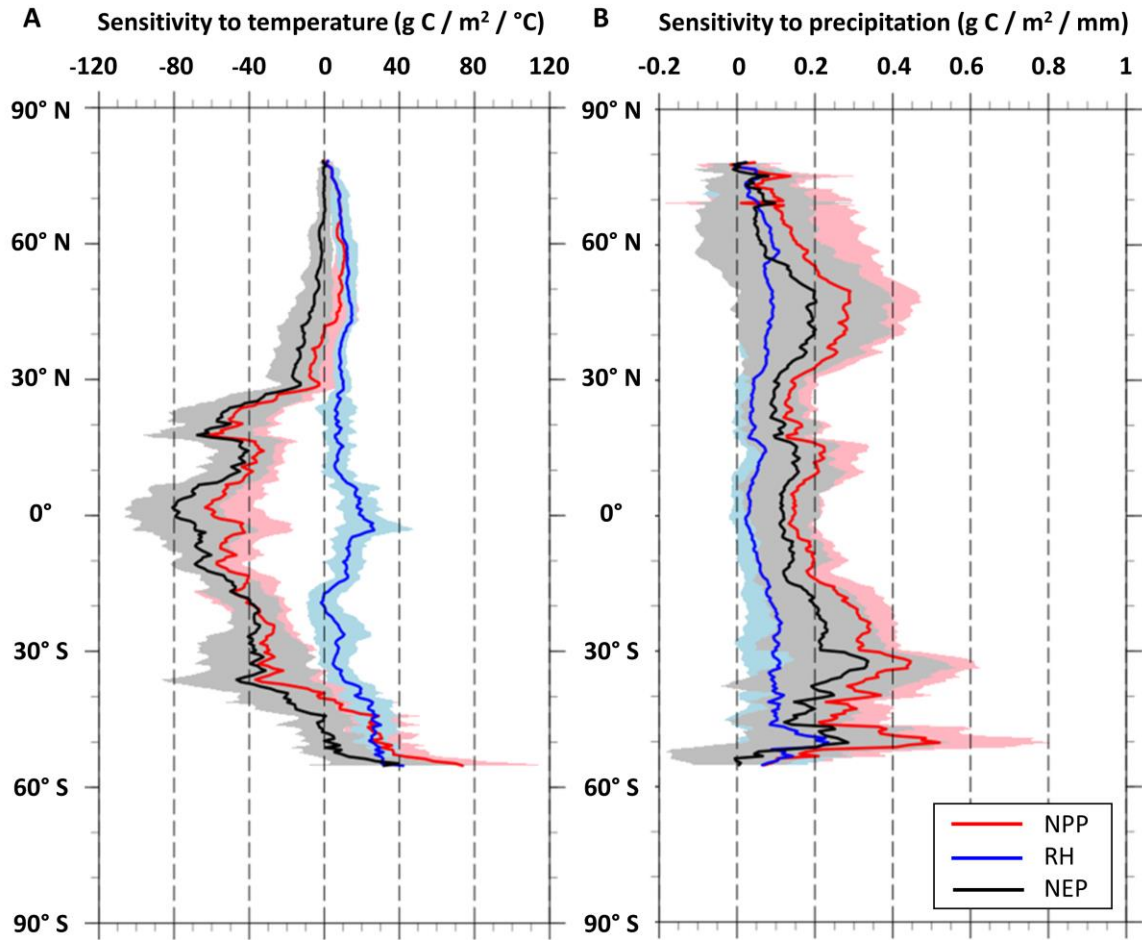


**Figure 3.** Latitudinal patterns of the sensitivity of carbon fluxes (NPP, Rh, and NEP) to (A) mean annual temperature and (B) mean annual precipitation. Shaded areas indicate the  $\pm 1$  standard deviation (SD) of the 19 model simulations.

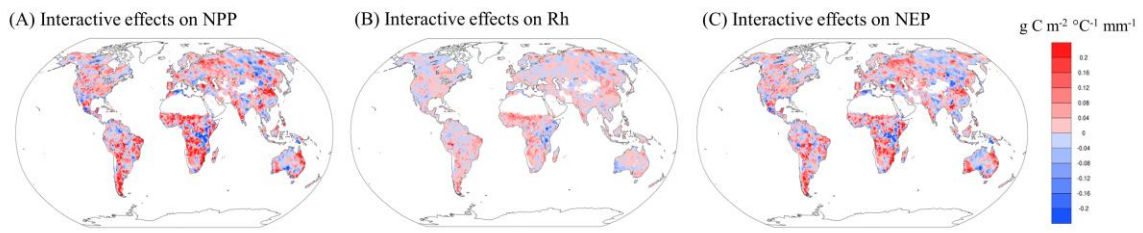


**Figure 4.** Interactive effects of temperature and precipitation on NPP (A), Rh (B), and NEP (C). Stippling indicates locations where over 75% of the simulations have the same sign (positive or negative) of the interactive effects (not clear in the figure due to small area).

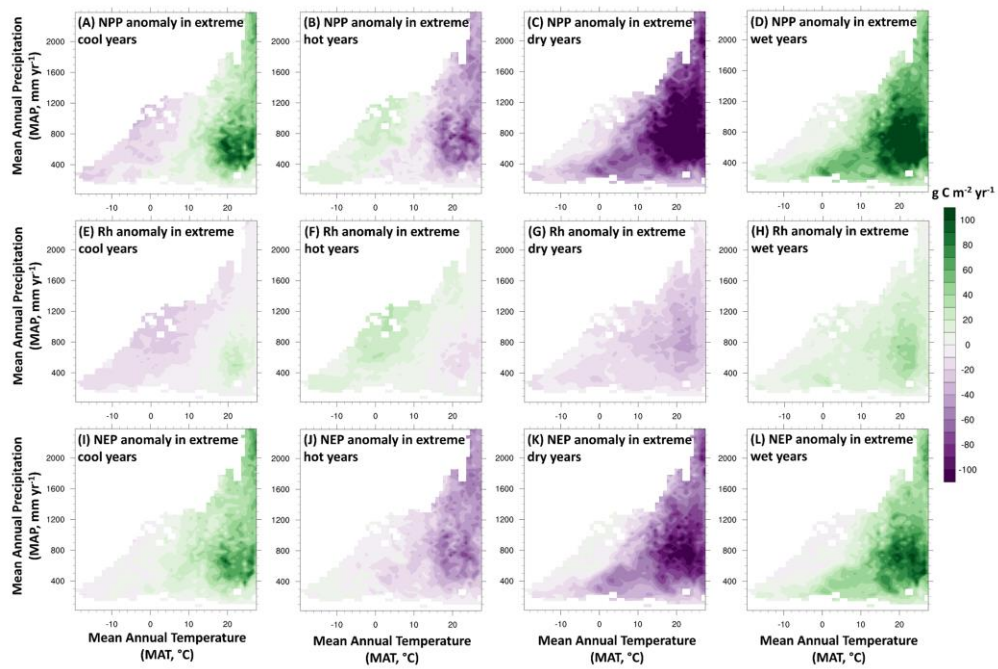


**Figure 5.** Anomalies of the terrestrial carbon fluxes. NPP (A-D), Rh (E-H), and NEP (I-L) during the extremely cold (A, E, I), hot (B, F, J), dry (C, G, K), and wet (D, H, L) years in climate space [x-axis: mean annual temperature (MAT), and y-axis: mean annual precipitation (MAP)].

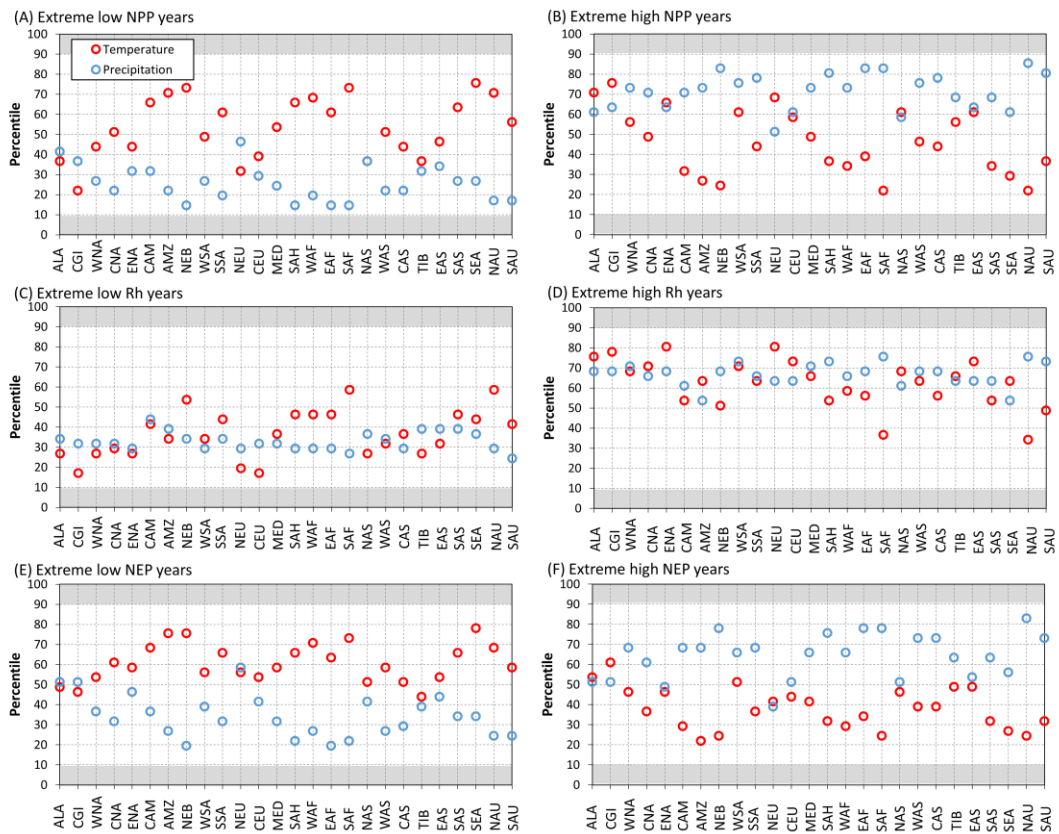


**Figure 6.** Percentiles of annual temperature and precipitation anomalies during the extreme low and high carbon years (A-B: NPP, C-D: Rh, E-F: NEP). x-axis refers to the 26 regions (see figure 1). The shaded area indicates the extreme climate events (10<sup>th</sup> and 90<sup>th</sup> percentiles).

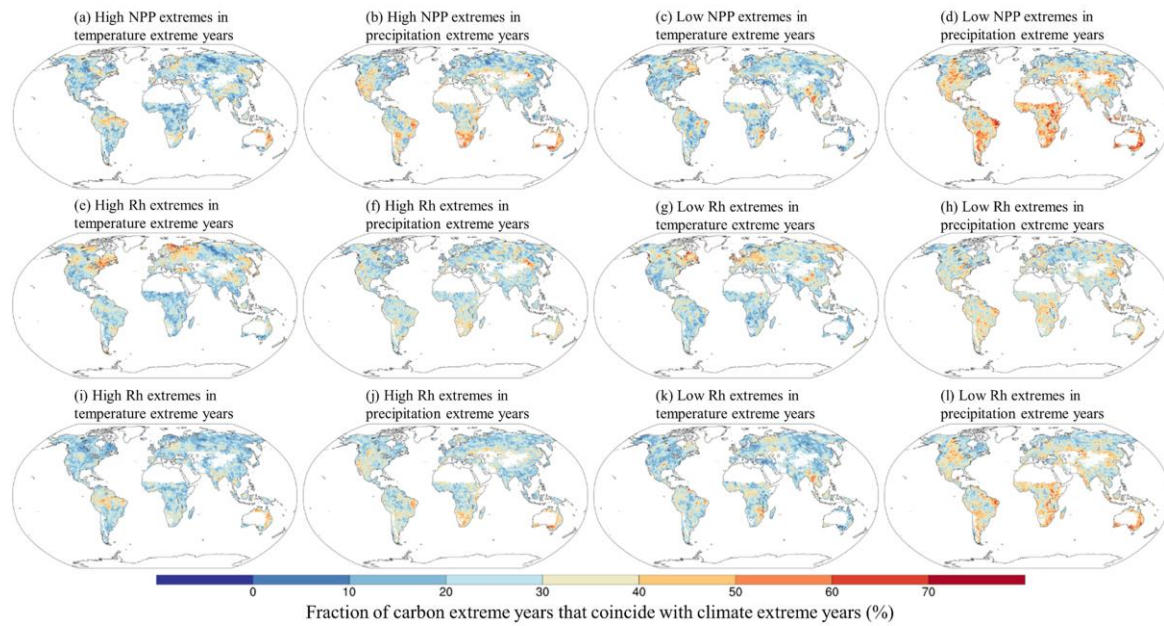


**Figure 7.** Fraction of carbon extreme years that coincide with climate extreme years (%). (a, b) High NPP extreme years in temperature and precipitation extreme years, (c, d) low NPP extreme years in temperature and precipitation extreme years, (e, f) high Rh extreme years in temperature and precipitation extreme years, (g, h) low Rh extreme years in temperature and precipitation extreme years, (i, j) high NEP extreme years in temperature and precipitation extreme years, (k, l) low NEP extreme years in temperature and precipitation extreme years. Temperature extreme years refer to both extreme hot and cool years, and precipitation extreme years refer to both extreme wet and dry years.

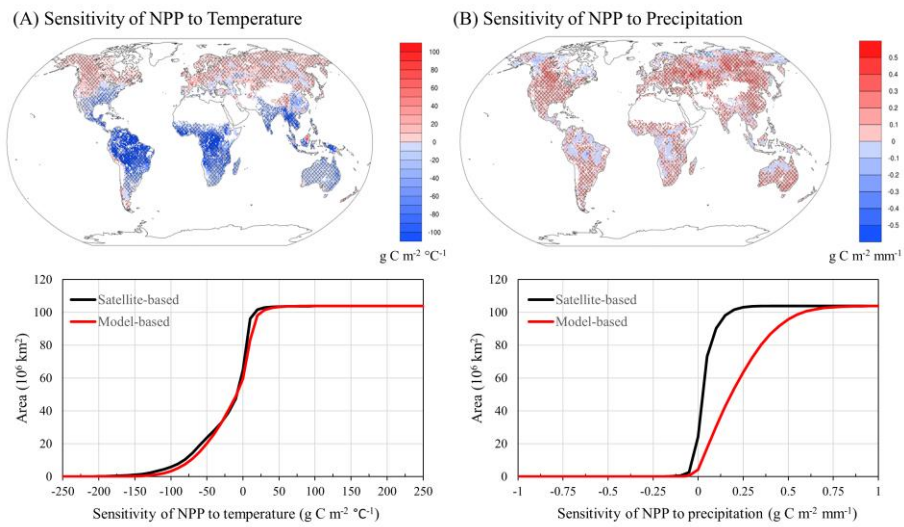


**Figure 8.** Sensitivity of satellite-based NPP to temperature (A) and precipitation (B), and the comparison with model-ensemble-based NPP sensitivity. Stippling indicates locations where satellite-based sensitivity and model-ensemble-based sensitivity agree on the sign.